ADVANCED ENERGY MATERIALS
www.advmat.de

Hydrogen Storage in Metal–Organic Framework

By *Yun Hang Hu** and *Lei Zhang*

Metal–organic frameworks (MOFs) are highly attractive materials because of their ultra-high surface areas, simple preparation approaches, designable structures, and potential applications. In the past several years, MOFs have attracted worldwide attention in the area of hydrogen energy, particularly for hydrogen storage. In this review, the recent progress of hydrogen storage in MOFs is presented. The relationships between hydrogen capacities and structures of MOFs are evaluated, with emphasis on the roles of surface area and pore size. The interaction mechanism between H_2 and MOFs is discussed. The challenges to obtain a high hydrogen capacity at ambient temperature are explored.

1. Introduction

An effective hydrogen-storage technology that provides a high storage capacity and fast kinetics is a critical factor in the development of a hydrogen fuel for transportation. Hydrogen can be stored in three ways: liquefaction, compressed hydrogen, and storage in a solid material.[1–7] The large amount of energy consumed during liquefaction and the continuous boil-off of hydrogen limit the possible use of liquid-hydrogen storage technology.[1] Compressing hydrogen is also an energy-consuming process and requires a very high pressure to obtain enough hydrogen fuel for a reasonable driving cycle of 300 miles, which in turn leads to safety issues related to tank rupture in case of accidents.[2] Therefore, current attention is focused on solid storage materials.[8,9] The storage of hydrogen in solid materials can be achieved by one of three processes: i) chemical reactions, in which hydrogen reacts with the solid material to form new compounds, ii) adsorption, in which hydrogen is adsorbed onto the solid material, and iii) cage occupancy, in which hydrogen is captured by cages. Materials for the storage of hydrogen through chemical reactions include metals, complex hydrides, and nitrides.[3–6b] These materials with relatively high hydrogen-storage capacities usually have a hydrogen-releasing temperature over 373 K (most even higher than 473 K) as a consequence of the high energy required to break chemical bonds. Such a high releasing temperature places a challenge on their applications for on-board hydrogen storage, for which the US Department of Energy (DOE) 2010 targets are hydrogen capacities of 6 wt% and 45 g H_2 L^{-1} and an operation temperature between 243 and 353 K. Hydrogen and H_2O can form clathrate hydrogen hydrates, in which hydrogen molecules are captured in H_2O cages.[10,11] The maximum hydrogen capacity is 5.3 wt% with current clathrate hydrates.[10] Furthermore, the introduction of tetrahydrofuran (THF) guest molecules can extremely reduce the pressure of hydrogen hydrate formation from 2200 to 50 bar.[11] However, to achieve a H_2 capacity of 6 wt% or higher, new structures of hydrogen hydrates are needed. Porous materials with high surface areas, such as activated carbon, nanotubes, and zeolites, have been widely investigated for hydrogen storage by adsorption.[12–14] The temperature of hydrogen release is usually low with these porous materials. However, they have low hydrogen capacities.

Over the last 30 years, the science of porous materials has become one of the most challenging issues for chemists and physicists.[15] Along with the progress of inorganic porous solids, the innovation for the synthesis of hybrid porous materials emerged at the beginning of the 1990s with the self-assembly of inorganic metal cations with organic linkers to form a network in the appropriate topology.[16–21] Such metal–organic frameworks (MOFs) attracted much attention because of their unusual structure and properties as well as their potential applications.[20,22] In 1997, Kitagawa et al. first reported gas adsorption on MOFs.[23] In 2003, Yaghi et al. first explored MOFs as H_2 storage materials.[24] Since that time, MOFs have become one of the most promising hydrogen-storage materials. Furthermore, MOFs are proving successful for hydrogen adsorption at 77 K. Currently, an exciting challenge for MOFs is to reach a high hydrogen capacity at ambient temperature with an acceptable pressure. There are several excellent review articles about MOFs for hydrogen storage,[25–30] which analyzed the effects of metal cluster and organic ligand structures, evaluated relationships between hydrogen capacities and surface areas (and pore sizes), and discussed strategies to improve hydrogen-storage capacity. Here, we review the recent progress in this rapidly developing field, with emphasis on the efforts and challenges to reach high hydrogen uptake in MOFs at ambient temperature and the interaction mechanism between hydrogen and MOFs.

2. Hydrogen Storage in MOFs at a Low Temperature of 77 K

The critical factors that determine hydrogen adsorption and desorption are the surface area of the adsorbents and the

[*] Prof. Y. H. Hu, L. Zhang
Department of Materials Science and Engineering
Michigan Technological University
Houghton, MI 49931-1295 (USA)
E-mail: yunhangh@mtu.edu

DOI: 10.1002/adma.200902096

Final page numbers not assigned

interaction between hydrogen and the adsorbents. At a low temperature of 77 K, hydrogen uptake on MOFs mainly depends on their total surface areas, particularly at high pressure. So far, various inorganic metal cations and organic linkers have been explored to tune the structure, pore size, and surface area of MOFs for hydrogen adsorption (Table 1).

2.1. Zn-Based MOFs

In 2003, Yaghi et al. reported an interesting MOF material (MOF-5, Fig. 1a) with hydrogen-sorption capacities.[24] MOF-5 has a crystal structure where inorganic $[Zn_4O]^{6+}$ groups are joined to an octahedral array of benzene-1,4-dicarboxylate (BDC) groups to form a porous cubic $Zn_4O(BDC)_3$ framework. Such a special structure is ideal for gas absorption because of its isolated linkers, which are accessible from all sides to the sorbate gas molecules. The scaffolding-like nature of MOF-5 and its derivatives led to extraordinarily high apparent surface areas (above 2000 m^2 g^{-1}). At 77 K and 0.7 bar, 4.5 wt% hydrogen absorption was obtained by using MOF-5.[24] This work prompted numerous investigations into storing hydrogen in MOF materials.[25,31–42] Although the 4.5 wt% hydrogen capacity of MOF-5 at 0.7 bar and 77 K was revised and attributed to the adsorption of some impurity gases,[37] its maximum hydrogen capacity of 4.5–5.2 wt% has been confirmed at 77 K and about 50 bar by three independent groups.[35,39,40] Furthermore, by evaluating MOF-5 derivatives composed of the same inorganic $[Zn_4O]^{6+}$ groups and different organic linkers,[35] Yaghi et al. found that the maximum H_2 uptakes in MOFs correlate well with surface areas. Among these MOFs, MOF-177 (Fig. 1c) with the highest apparent surface area (Brunauer–Emmett–Teller (BET) surface area: 4746 m^2 g^{-1}) had the highest hydrogen uptake of 7.5 wt% at 77 K and 70 bar (Fig. 2).[35]

The preparation approaches for MOFs can have effects on their hydrogen adsorption capacities. Yaghi et al. reported that the hydrogen-storage capacity of MOF-5 was variable with synthesis and handling conditions. The maximum H_2 uptakes of MOF-5 samples prepared with and without exposure to air were 5.1 and 7.1 wt%, respectively.[36] The N_2 adsorption measurements showed that the exposure in air led to a reduction in its BET surface area from 3800 to 3100 m^2 g^{-1}, confirming the deleterious effects of air exposure. This discrepancy was attributed to the decomposition of $Zn_4O(BDC)_3$ in humid air. They found that exposure of a pulverized and desolvated sample of $Zn_4O(BDC)_3$ to air for 10 min resulted in the appearance of a new peak at $2\theta = 8.9^\circ$ in the powder X-ray diffraction (XRD) pattern, suggesting the partial conversion in a second phase (Fig. 3).[36] Furthermore, when the sample was further exposed to air, they observed an increase in the relative intensity of this XRD peak and the appearance of two additional peaks at $2\theta = 15.8^\circ$ and 17.8°, indicating the formation of a compound isostructural to $Zn_3(OH)_2(BDC)_2 \cdot 2DEF$ (DEF = *N*,*N*-diethylformamide) (MOF-69C). After exposure to air for 24 h, $Zn_4O(BDC)_3$ was converted into a solid of formula $C_{24}H_{22}O_{18}Zn_4$. In contrast, the structure of $Zn_4O(BDC)_3$ was not affected by exposing to dry O_2 or anhydrous organic solvents such as methanol, *N*,*N*-dimethylformamide (DMF), and dimethyl sulfoxide (DMSO). Very recently, Hafizovic et al. studied the structural difference between low and high surface area MOF-5 samples, which are dependent on preparation approach.[43] The low surface area MOF-5 had two types of crystals. In the dominant phase, the $Zn(OH)_2$ species, which partly occupied the cavities, makes the hosting cavity and adjacent cavities inaccessible, which leads to a reduction in the pore volume and the effective surface area of the material. Furthermore, the minor phase consisted of doubly interpenetrated MOF-5 networks, which lowers the adsorption capacity. Thus, the hydrogen adsorption capacity of $Zn_4O(BDC)_3$, which is determined by surface area, strongly depends on preparation conditions. This can explain the difference in hydrogen-adsorption capacities reported for $Zn_4O(BDC)_3$ from various groups (Table 1).[19,36–42]

The effect of Pd on hydrogen storage in MOF-5 was examined by Sabo et al.[44] Although the surface area of MOF-5 decreased from 2885 to 958 m^2 g^{-1} by supporting Pd on it, its hydrogen-adsorption capacity increased from 1.15 to 1.86 wt% at 77 K and 1 bar. This happened probably because Pd can increase the hydrogen adsorption energy, which determines the hydrogen capacity at a low pressure.

The intergrowth of two or more frameworks can also affect their properties for hydrogen storage. As shown in Figure 4, one can see that, compared with non-interpenetrating MOFs, the

Yun Hang Hu received his Ph.D. in physical chemistry from Xiamen University. He was Assistant Professor and Associate Professor at Xiamen University, Senior Staff Engineer at the ExxonMobil Research and Engineering Company, and Research Full Professor of Chemical and Biological Engineering at the State University of New York at Buffalo. Currently, he is an assistant professor of materials science and engineering at Michigan Technological University. His main research interests range from hydrogen-storage materials, nanostructured materials, CO_2 conversion, catalysis, surface science, quantum chemistry, to solar energy.

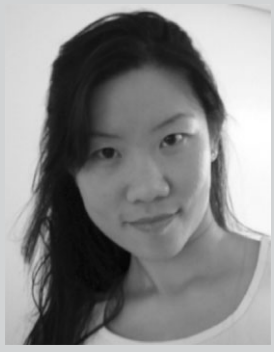

Lei Zhang is currently pursuing her Ph.D. in materials science and engineering in the group of Prof. Y. H. Hu. Her current research involves the synthesis, characterization, and application of metal-organic frameworks. She received her B.Sc. and M.Sc. in materials science and engineering from China University of Mining and Technology (Beijing).

Table 1. Summary of hydrogen adsorption on MOFs at 77 K.

Materials[a]	Apparent surface area [b] [m^2 g^{-1}]	Heat of adsorption [kJ mol^{-1}]	H_2 uptake [i] [wt%]	Pressure [bar]	Ref.
$Zn_4O(BDC)_3$, MOF-5 or IRMOF-1	2000	/	4.5	0.7	[24]
	3362, 2900 [c]	/	1.32	1	[37]
	2296 [c]	−3.8/−4.8 [f]	4.7	50	[38–40]
	/	/	3.6	10	[39]
	3100 [c]	/	5.1	40	[36]
	/	/	4.1	10	[36]
	3800 [c]	/	7.1	50	[36]
	/	/	5.1	10	[36]
	570, 47 [c]	/	0.2	10	[42]
	1014, 572[c]	/	1.6	10	[42]
$Zn_4O(C_8H_3BrO_4)_3$, IRMOF-2	2544, 1722 [c]	/	1.2	1	[38]
$Zn_4O(C_8H_5NO_4)_3$, IRMOF-3	3563	/	1.4	1	[111]
	3062, 2446 [c]	/	1.4	1	[38]
$Zn_4O(C_{14}H_8O_4)_3$, IRMOF-9	2631,1904 [c]	/	1.2	1	[38]
$Zn_4O(C_{18}H_8O_4)_3$, IRMOF-13	2100,1551 [c]	/	1.7	1	[38]
$Zn_4O(R^6\text{-}BDC)_3$, IRMOF-6	3300	/	4.8 (31) [j]	50	[35]
	3263,2476 [c]	/	1.5	1	[38]
$Zn_4O(NDC)_3$, IRMOF-8	1466	/	1.50	1	[37]
	1466	−6.1 [f]	1.50	40	[35,40]
$Zn_4O(HPDC)_3$, IRMOF-11	1911	/	1.62	1	[37]
	2340	−9.1 [f]	3.5 (27) [j]	35	[35]
$Zn_4O(TMBDC)_3$, IRMOF -18	1501	/	0.89	1	[37]
$Zn_4O(TTDC)_3$, IRMOF-20	4590	/	6.7 (34)[j]	70	[35]
	4346,3409 [c]	/	1.4	1	[38]
$[Zn_4O(NTB)_2]\cdot 3DEF\cdot EtOH$	1121	/	1.9	1	[49]
$Zn_4O(BTB)_2$, MOF-177	4526	/	1.25	1	[37]
	4746 [c]	/	7.5 (32) [j]	70	[35]
$Zn_2(BDC)_2(DABCO)$	1450 [c]	/	2.0	1	[46]
	2090,1450 [c]	/	2.0	1	[50]
$Zn_2(BDC)(TMBDC)(DABCO)$	1670,1100 [c]	/	2.1	1	[50]
$Zn_2(TMBDC)_2(DABCO)$	1400,920 [c]	/	1.9	1	[50]
$Zn_2(NDC)_2(DABCO)$	1450,1000 [c]	/	1.7	1	[50]
$Zn_2(TFBDC)_2(DABCO)$	1610,1070 [c]	/	1.8	1	[50]
$Zn_2(TMBDC)_2(BPY)$	1740,1120 [c]	/	1.7	1	[50]
$[Zn(BDC)(TED)_{0.5}]\cdot 2DMF\cdot 0.2H_2O$	/	/	2.1	1	[48]
Zn(TBIP)	256	−6.7 to −6.4[f]	0.75	1	[118]
$Zn_2(C_8H_2O_6)$, MOF-74	1132,783 [c]	−8.3[f]	1.8	1	[38]
$[Zn_3(BPDC)_3BPY]\cdot 4DMF\cdot H_2O$	792 [c]	−7.2[f]	1.74	1	[51]
$Zn_3(BDT)_3$	640 [c]	−6.8 to −8.7 [f]	1.46	1	[57]
$[Co_3(BPDC)_3BPY]\cdot 4DMF\cdot H_2O$	922 [c]	−6.8 [f]	1.98	1	[51]
Al(OH)(BDC), MIL-53(Al)	1590,1020[c]	/	3.8	16	[67,70]
Cr(OH)(BDC), MIL-53(Cr)	1500,1026 [c]	/	3.1	16	[67,70]
$[Mn(DMF)_6]_3[(Mn_4Cl)_3(BTT)_8(H_2O)_{12}]_2\cdot 42DMF\cdot 11H_2O\cdot 20CH_3OH$	1100[c]	−7.6[f]	3.9 (35) [j]	50	[66]
$[Mn(DMF)_6]_3[(Mn_4Cl)_3(BTT)_8(H_2O)_{12}]_2\cdot 42CH_3OH$	2100 [c]	−10.1[f]	6.9 (60) [j]	90	[66]
$[Mn(NDC)]_n$	191	/	0.57	1	[65]
$Mn(HCO_2)_2$	297 [d]	/	0.9	1	[25]
$Mn_3(BDT)_3$	290 [c]	−6.3 to −8.4 [f]	0.97	1	[57]
$Mn_2(BDT)Cl_2$	530 [c]	−6.0 to −8.8 [f]	0.82	1	[57]
$Cu_2(BPTC)$, MOF-505	1646	/	2.48	1	[53]
	1670 [c]	/	4.02 (37) [j]	20	[54]
$Cu_2(TPTC)$	2247 [c]	/	6.06 (39) [j]	20	[54]
$Cu_2(QPTC)$	2932 [c]	/	6.07 (36) [j]	20	[54]
$Cu_3(BTC)_2$, HKUST-1	1958	−4.5/−6.8 [f]	3.6	50	[38,39]
	/	/	2.5	1	[39]
	1482 [c]	/	4.1	26	[63]
	/	/	2.9	1	[63]
	/	/	0.66	1	[57]
	1239 [c]	−6.1 [f]	2.18	1	[59]

Final page numbers not assigned

Table 1. Continued

Materials[a]	Apparent surface area [b] [m^2 g^{-1}]	Heat of adsorption [kJ mol^{-1}]	H_2 uptake [i] [wt%]	Pressure [bar]	Ref.
	2175,1507 [c]	−6.9 [f]	2.5	1	[38]
$Cu_3(TATB)_2(H_2O)_3$	3800	/	1.91	1	[51]
$Zn_3(BDC)_3[Cu(PYEN)]\cdot(DMF)_5(H_2O)$	/	/	0.2	10	[64]
Ni(cyclam)(BPYDC)	817	/	1.1	1	[72]
$Ni_2(BPY)_3(NO_3)_4$ (M)	/	/	0.8	1	[33]
$Ni_2(BPY)_3(NO_3)_4$ (E)	/	/	0.7	1	[33]
$Ni_3(BTC)_2(3\text{-}PIC)_6(PD)_3$	/	/	2.1	1	[33]
$Sc_2(C_8H_4O_4)_3$	721 [c]	/	1.5	0.8	[78]
$M_3[Co(CN)_6]_2$ M = Mn, Fe, Co, Ni, Cu, Zn	720–870 [c]	−5/−7.4 [f]	1.4–1.8	1	[79]
$Mg_3(NDC)_3$	190 [e]	−7/−9.5 [f]	0.48	1	[80]
$Al_3O(OH)(BTC)_3$, MIL-96(Al)	/	/	1.91	3	[69]
$COF(BTC)_2$, MIL-100(Cr)	2700	−5.6/−6.3 [g]	3.3	27	[71]
$Cr_3OF(BDC)_3$, MIL-101(Cr)	5500	−9.3/−10.0 [g]	6.1	60	[71]
$Cr_3OF(NTC)_{1.5}$, MIL-102(Cr)	42	−5.99 [h]	1.0	35	[68]
	/	/	0.05	35	[68]
$NaNi_3(OH)(SIP)_2$	/	−9.4 to −10.4 [f]	0.94 [h]	1	[74]

[a] Acronyms: BDC = benzene-1,4-dicarboxylate; R^6-BDC = 1,2-dihydrocyclobutylbenzene-3,6-dicarboxylate, NDC = naphthalene-2,6-dicarboxylate; HPDC = 4,5,9,10-tetrahydropyrene–2,7-dicarboxylate; TMBDC = 2,3,5,6-tetramethylbenzene-1,4-dicarboxylate; TTDC = thieno[3,2-b]thiophene-2,5-dicarboxylate; NTB = 4,4′,4″-nitrilotrisbenzoate; BTB = benzene-1,3,5-tribenzoate; DEF = *N*,*N*′-diethylformamide; DABCO = 1,4-diazabicyclo[2.2.2]octane; TFBDC = tetrafluoroterephthalate; TED = triethylenediamine; DMF = *N*,*N*-dimethylformamide; TBIP = 5-tert-butyl isophthalate; BPDC = biphenyldicarboxylate; BPY = 4,4′-bipyridine; BDT = 1,4-benzeneditetrazolate; BPTC = biphenyl-3,3′,5,5′-tetracarboxylate; TPTC = terphenyl 3,3″:5,5″-tetracarboxylate; QPTC = quaterphenyl 3,3‴;:5,5‴;-tetracarboxylate; BTC = benzene-1,3,5-tricarboxylate; TATB = 4,4′,4″-s-triazine-2,4,6-triyltribenzoate; $PYENH_2$ = 5-methyl-4-oxo-1,4-dihydro-pyridine-3-carbaldehyde CYCLAM = 1,4,8,11-tetraazacyclotetradecane; BPYDC = 2,2′-bipyridyl-5,5′-dicarboxylate; 3-PIC = 3-picoline; PD = propane-1,2-diol; SIP = 5-sulfoisophthalate. Calculated from N_2 adsorption at 77 K using the Langmuir model except where indicated. [c] BET surface area from N_2 adsorption at 77 K. [d] BET surface area from CO_2 adsorption at 195 K. [e] BET surface area from O_2 adsorption at 77 K. [f] Values obtained from adsorption experiments at different temperatures. [g] Value obtained from microcalorimetric experiments at low coverage. [h] Values deduced from simulations. [i] Gravimetric uptake of hydrogen (wt%) except where indicated. [j] Volumetric uptake of hydrogen (g H_2 L^{-1}).

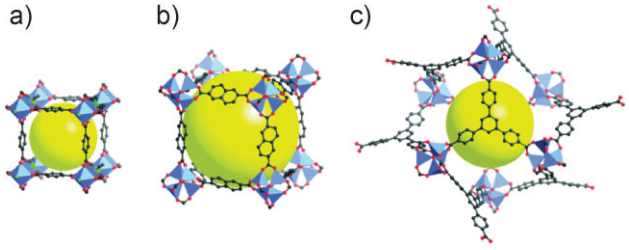

Figure 1. MOFs: a) MOF-5, $Zn_4O(BDC)_3$, b) IRMOF-8, $Zn_4O(NDC)_3$, and c) MOF-177, $Zn_4O(BTB)_2$. Reproduced with some modifications from ref. [25].

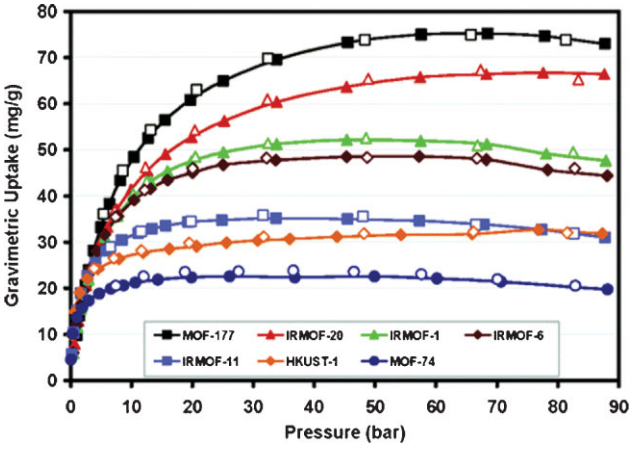

Figure 2. Hydrogen isotherms for the activated materials measured at 77 K in gravimetric units (mg g^{-1}). Filled markers represent adsorption, open markers denote desorption. Reproduced with permission from ref. [35]. Copyright 2006, American Chemical Society.

interwoven IRMOF-11 material showed the greatest hydrogen uptake at 77 K and pressure below 800 torr (1.07 bar).[37] This happened because catenation can reduce the free diameter of pores.[25,45,46]

A series of dinuclear paddlewheel-structured MOFs were explored.[47–49] Dybtsev et al.[47] synthesized a paddlewheel-structured $[Zn_2(BDC)_2(DABCO)]\cdot 4DMF\cdot 0.5H_2O$ (DABCO = 1,4-diazabicyclco[2.2.2]octane). The framework is composed of dinuclear Zn_2 units with a paddlewheel structure, which are bridged by BDC dianions to form a distorted 2D square-grid $[Zn_2(BDC)_2]$. The axial sites of the Zn_2 paddlewheels are occupied by DABCO acting as pillars to extend the 2D layers into a 3D structure (Fig. 5). Although BDC is generally considered to be a linear and rigid linker, the linker in this structure is bent, leading to severe twisting of the Zn_2 paddlewheel from an ideal square grid. Interestingly, after evacuation of guest molecules, the BDC ligands linking the Zn_2 paddlewheel units became linear, which resulted in a perfect 2D square grid of $[Zn_2(BDC)_2]$. Such a

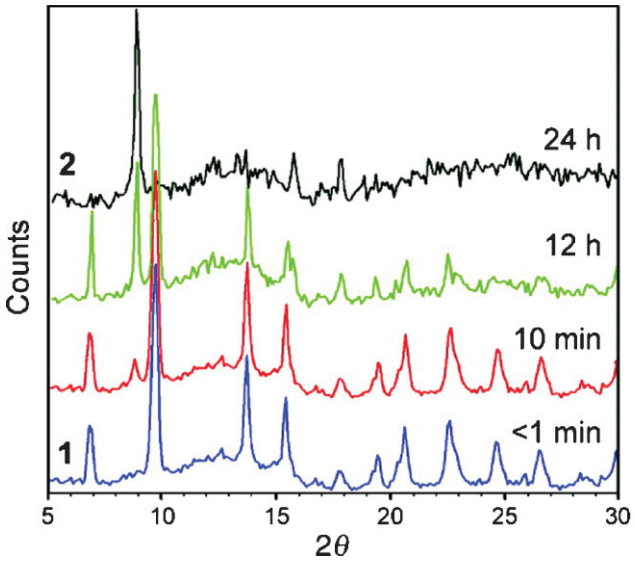

Figure 3. Powder XRD patterns collected using Cu Kα radiation for $Zn_4O(BDC)_3$ exposed to air for <1 min (1), 10 min, 12 h, and 24 h (2). The broad hump centered at ca. 13° is due to the sample holder. Reproduced with permission from ref. [36]. Copyright 2007, American Chemical Society.

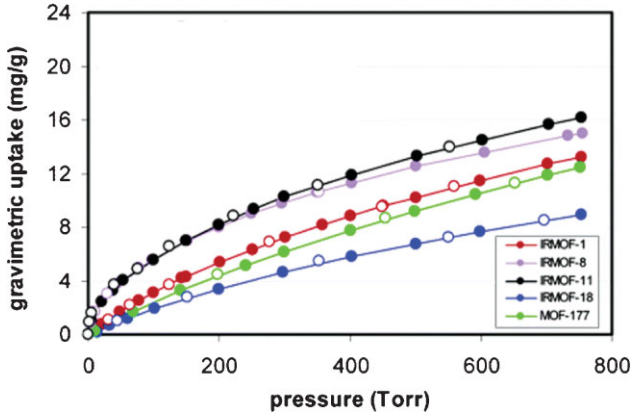

Figure 4. Hydrogen isotherms for the activated materials measured gravimetrically at 77 K. Filled maskers: adsorption; open maskers: desorption. Reproduced with permission from ref. [37]. Copyright 2004, American Chemical Society.

paddlewheel-structured MOF, which has a high BET surface area of 1450 m^2 g^{-1}, exhibited an adsorption capacity of 2.0 wt% at 77 K and 1 bar. Furthermore, Chun et al. combined various aromatic dicarboxylates,[50] including BDC, tetramethylterephthalate (TMBDC), 1,4-naphthalenedicarboxylate (1,4-NDC), tetrafluoroterephthalate (TFBDC), 2,6-naphthalenedicarboxylate (2,6-NDC), DABCO, and 4,4′-dipyridyl (BPY), to form paddlewheel-structured frameworks $[Zn_2(BDC)_2(DABCO)]$, $[Zn_2(BDC)(TMBDC)(DABCO)]$, $[Zn_2(TMBDC)_2(DABCO)]$, $[Zn_2(1,4\text{-NDC})_2(DABCO)]$, $Zn_2(TFBDC)_2(DABCO)]$, and $[Zn_2(TMBDC)_2(BPY)]$. These frameworks possess surface areas in the range of 1450–2090 m^2 g^{-1} and hydrogen-adsorption capacities of 1.7–2.1 wt% at 77 K and 1 bar. In addition, using BDC,

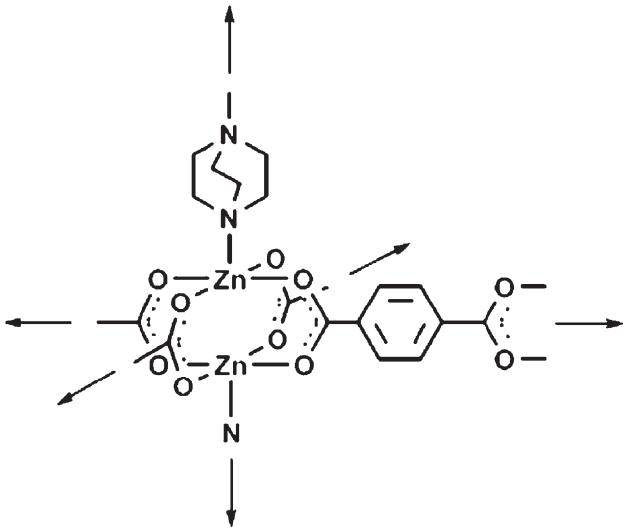

Figure 5. The extension of the 2D square-grid of $\{Zn_2(1,4\text{-BDC})_2\}$ into a 3D structure by using DABCO, which occupies the axial positions. Reproduced from ref. [47].

triethylenediamine (TED), and DMF, Lee et al.[48] synthesized the framework $[Zn(BDC)(TED)_{0.5}]\cdot 2DMF\cdot 0.2H_2O$. This framework, which also possesses a paddlewheel structure, adsorbed 2.1 wt% of hydrogen at 77 K and 1 bar. These results indicate that paddlewheel-structured dinuclear Zn-based MOFs have almost the same hydrogen capacity, which indicates that the type of organic linker does not have an obvious effect on the hydrogen uptake of a paddlewheel-structured Zn-based MOF.

Lee et al. examined hydrogen adsorption on a trinuclear framework $[Zn_3(BPDC)_3BPY]\cdot 4DMF\cdot H_2O$ (BPDC = biphenyldicarboxylate).[51] The structure of the framework possesses two crystallographically independent zinc centers (Zn1 and Zn2). Two Zn1 atoms and one Zn2 atom form a trinuclear metal cluster $[Zn_3(BPDC)_6(BPY)_2]$, in which one octahedral metal (Zn2) is located at the center and two tetrahedral metals (Zn1) are situated at two ends. The metal nodes are connected to adjacent nodes by carboxylate groups from six BPDC ligands located in the equatorial plane to form 2D double layers. The remaining two apical positions of the Zn1 are bound to the nitrogen atoms of BPY to form a 3D pillared framework. As a result, its BET surface area is 792 m^2 g^{-1}. Furthermore, the hydrogen-adsorption measurements showed that it could adsorb 1.74 wt% of H_2 at 77 K and 1 bar. The high density of adsorbed H_2 falls in the range of liquid H_2, which suggests relatively strong sorbent–sorbate interactions in the material.

2.2. Cu-Based MOFs

The synthesis of copper(II)-based MOFs also attracted much attention.[38,39,52–61] The first Cu–organic framework is HKUST-1 (also called CuBTC, where BTC = 1,3,5-benzene tricarboxylate), which was invented by Williams et al.[52] and subsequently studied by numerous research groups.[38,39,53–57] HKUST-1, which is composed of Cu^{II} paddlewheel clusters linked by trigonal benzene-1,3,5-tricarboxylate, possesses a face-

centered- cubic crystal that contains an intersecting 3D system of a bimodal pore size distribution with a BET surface area of about 1500 $m^2 g^{-1}$. The advantage of using copper(II) is that its property toward John–Teller distortion weakens the bonding of nucleophiles (such as solvent molecules) at the axial sites. The removal of these species can create the open metal sites and the $Cu^{\delta+}$–$O^{\delta-}$ dipoles on the surface, which leads to an increase in the local interaction energy for hydrogen or other adsorptives. Indeed, the isosteric heat of hydrogen adsorption at low coverage is 1–2.0 kJ mol^{-1} larger for HKUST-1 than for MOF-5.[38,39] As a result, the amount of H_2 adsorbed by HKUST-1 at 1 bar and 77 K was approximately double that of MOF-5.[39,46] However, at higher pressures, MOF-5 had a much higher H_2 adsorbed amount than HKUST-1. This occurred because the adsorbed hydrogen amount at low pressure strongly depends on the binding strength of H_2 to the frameworks, whereas the amount adsorbed at higher pressure is mainly determined by the surface area.[62] Furthermore, the preparation and activation processes can have a significant impact on hydrogen adsorption capacity, surface area, and pore volume of HKUST-1.[63] The H_2 uptakes on HKUST-1, which were measured by different groups under nominally the same conditions, vary considerably for two possible reasons: crystal defects and the presence of guest molecules (contaminants) in the HKUST-1 samples.[63] For example, Liu et al. found the removal of all solvent from HKUST-1 by an improved activation process can increase its maximum hydrogen uptake up to 4.1 wt% at 26 bar and 77 K.[63]

Yaghi et al. reported a new Cu–organic framework, $[Cu(L^1)(H_2O)_2]$ (L^1 = biphenyl-3,3′,5,5′-tetracarboxylic).[53] The framework (referred to as MOF-505) has a crystal structure in which Cu^{II} is coordinated by five O atoms in a square pyramidal geometry. Pairs of Cu^{II} centers are bridged by four carboxylate groups to form $[Cu_2(O_2CR)_4]$ paddlewheel units. A H_2O molecule binds to each Cu center along the paddlewheel axis. Each $[Cu_2(O_2CR)_4]$ paddlewheel is linked to four biphenyl liagnds and vice versa. After activation at 393 K, MOF-505 with a surface area of 1830 $m^2 g^{-1}$ can reversibly adsorb 2.47 wt% of H_2 at 77 K and 1 bar.[53] This adsorbed amount is comparable to that of HKUST-1. When the H_2 pressure increased to 20 bar, the uptake of hydrogen on MOF-505 reached 4.02 wt%.[54] To examine the effects of organic linkers, Lin et al. replaced the biphenyl-3,3′,5,5′-tetracarboxylic (L^1) of MOF-505 with the terphenyl-3,3″,5,5″-tetracarboxylic (L^2) and the quaterphenyl-3,3‴, 5,5‴-tetracarboxylic (L^3), to form two new frameworks $[Cu_2(L^2)(H_2O)_2]$ (**1**) and $[Cu_2(L^3)(H_2O)_2]$ (**2**).[54] Frameworks **1** and **2** have higher surface areas of 2247 and 2932 $m^2 g^{-1}$, respectively. The pore sizes are narrowly distributed around 6.5, 7.3, and 8.3 Å for MOF-505, framework **1**, and framework **2**, respectively. At 1 bar (or below) and 77 K, MOF-505 had the highest hydrogen uptake, framework **2** the lowest, and framework **1** in between. However, when the pressure was above 2.5 bar, the H_2 uptake of the later two exceeded that of MOF-505. Furthermore, at 20 bar and 77 K, the H_2 uptakes of frameworks **1** and **2** reached 6.06 and 6.07 wt%, respectively. Fitting the high pressure region of their H_2 isotherms to the Langmuir equation gave a maximum adsorption of 4.2, 6.7, and 7.01 wt% of H_2 for MOF-505, framework **1**, and framework **2**, respectively.[54] This indicates that the hydrogen adsorption is dependent on the pore size (related to affinity for H_2) at a low pressure, whereas the surface area is a key factor in controlling the H_2 adsorption at a high pressure.

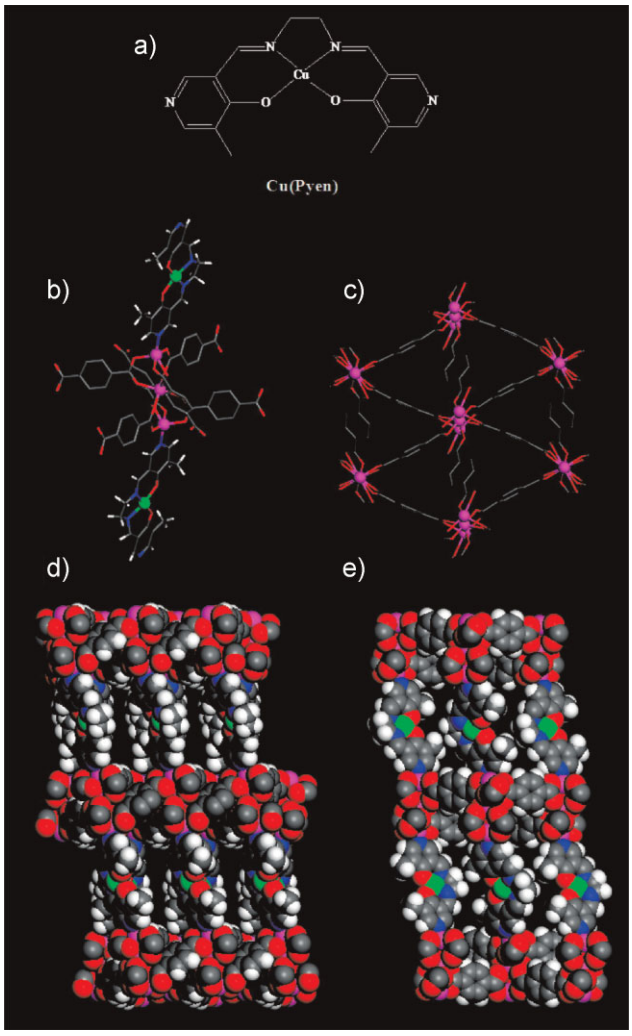

Figure 6. X-ray crystal structure of ($Zn_3(BDC)_3Cu(PYEN)$) showing a) PYEN, b) one trinuclear $Zn_3(COO)_6$ secondary building unit, c) one 3^6 tessellated $Zn_3(BDC)_3$ 2D sheet pillared by the Cu(PYEN), d) the curved pores of about 5.6 × 12.0 Å along the *c*-axis, and e) the irregular ultramicropores along the *b*-axis. Legend: Zn (magenta), Cu (green), O (red), N (blue), C (gray), H (white). Reproduced with permission from ref. [64]. Copyright 2008, American Chemical Society.

Zhou et al. reported the synthesis and structure of framework $Cu_3(TATB)_2(H_2O)_3$ (TATB = 4,4′,4″-*s*-triazine-2,4,6-triyltribenzoate).[58] Its structure possesses dicopper tetracarboxylate paddlewheel secondary building units (SBUs). With axial aqua ligands, which are linked by TATB bridges. This framework adsorbed about 1.9 wt% of hydrogen at 1 bar and 77 K.

Chen et al. successfully synthesized a mixed zinc/copper MOF $Zn_3(BDC)_3[Cu(PYEN)] \cdot (DMF)_5(H_2O)_5$ ($PYENH_2$ = 5-methyl-4-oxo-1,4-dihydro-pyridine-3-carbaldehyde) (Fig. 6).[64] Its desolvation generated a bimodal porous structure with narrow porosity (<0.56 nm) and an array of pores in the *bc*-crystallographic plane. In such a structure, the adsorbate–adsorbent interactions were maximized by both the presence of open copper centers and the overlap of the potential energy fields from pore walls.[64] Its

heat of hydrogen adsorption is about 12 kJ mol^{-1} (at zero surface coverage), which is the highest value so far observed for hydrogen adsorption on MOFs. However, this Cu/Zn hybrid MOF had a low hydrogen uptake of 0.2 wt% at 77 K and 10 bar because of its small surface area.

2.3. Mn-Based MOFs

Moon et al.[65] reported $[Mn(NDC)(DEF)]_n$, which is a 3D porous MOF generating 1D channels. $[Mn(NDC)(DEF)]_n$ has no free space, because the DEF molecules that coordinate the Mn^{II} ions occupy the channels. However, the DEF can be removed to obtain desolvated $[Mn(NDC)]_n$ that contains accessible coordination sites on Mn^{II} sites, which results in a surface area of 191 m^2 g^{-1} and a H_2 uptake of 0.57 wt% at 77 K and 1 bar.[65]

Long et al. synthesized a new Mn-based framework, $[Mn(DMF)_6]_3[(Mn_4Cl)_3(BTT)_8(H_2O)_{12}]_2 \cdot 42DMF \cdot 11H_2O \cdot 20CH_3OH$, by using the tritopic bridging ligand 1,3,5-benzenetristetrazolate (BTT^{3-}).[66] This porous MOF possesses a cubic topology.[66] Crystals of the compound with a high surface area up to 2100 m^2 g^{-1} showed a H_2 uptake of 6.9 wt% at 77 K and 90 bar. Furthermore, the H_2 uptake can further increase with pressure, because H_2 adsorption did not reach its saturation at 90 bar. Such a high hydrogen uptake was attributed to its high adsorption heat (10.1 kJ mol^{-1} at zero surface coverage), which was directly related to H_2 binding at coordinatively unsaturated Mn^{2+} centers within the framework.[66]

2.4. Cr or Al-Based MOFs

Several Cr- or Al-based MOFs have been evaluated for hydrogen storage (Table 1).[67–70] Férey et al.[67] investigated the hydrogen adsorption properties on the metal–benzenedicarboxylate $M(OH)(O_2C\text{-}C_6H_4\text{-}CO_2)$ [$M = Al^{3+}$ or Cr^{3+}] denoted as MIL-53 [MIL: material from Institute Lavoisier]. The frameworks exhibited 1D channels with large free diameters of about 8.5 Å and a large BET surface area of 1100 m^2 g^{-1}. The chromium compound showed a maximal hydrogen capacity of 3.1 wt% at 77 K and 16 bar, whereas the aluminum one exhibited the capacity of 3.8 wt%. Furthermore, they evaluated the hydrogen adsorption on the giant-pore Cr-based MIL-100 and MIL-101 (Fig. 7).[71] MIL-100 and MIL-101 were built up from carboxylate moieties (BTC for MIL-100 and BDC for MIL-101) and trimeric chromium(III) octahedral clusters that had removable terminal water molecules and, therefore, provided potential unsaturated metal sites in the structure. The smaller of the two types of cages in their architectures was delimited by 12 pentagonal faces and the larger by 16 faces (12 pentagonal and 4 hexagonal). Without guest molecules, the accessible diameters of the cages were 25 and 29 Å for MIL-100 and 29 and 34 Å for MIL-101. The MIL-100, which was previously outgassed at 493 K, had a Langmuir surface area of 2700 m^2 g^{-1} and a maximum hydrogen uptake of 3.28 wt% at 77 K and 26.5 bar. In the MIL-101a that was obtained by outgassing MIL-101 with the same approach as for MIL-100, a significant amount of $BDCH_2$ molecules was still within the pores, which implied that most of metal sites were still poisoned by $BDCH_2$ molecules. Its Langmuir surface was 4000 m^2 g^{-1}. At 77 K, the isotherm of hydrogen adsorption exhibited a maximum

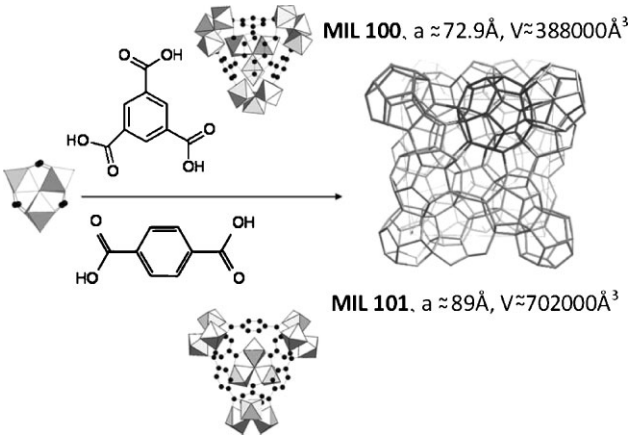

Figure 7. Schematic view of MIL-100 and MIL-101. Left: trimers of chromium octahedra that assemble with either BTC (MIL-100) or BDC (MIL-101) to form the hybrid supertetrahedra; right: the resulting zeotype architecture (each intersection of cages is occupied by a supertetrahedron). Reproduced from ref. [71].

capacity at 4.5 wt% with a saturation plateau above 40 bar. Furthermore, if MIL-101a was further subjected to additional treatment to evacuate most of the $BDCH_2$ in the pores, the resultant sample (denoted as MIL-101b) had only half of the metal sites that were poisoned by coordinated $BDCH_2$ molecules. Its Langmuir surface area was as large as 5500 m^2 g^{-1}. The maximum hydrogen adsorption capacity of MIL-101b reached 6.1 wt% at 80 bar and 77 K. The high adsorption capacity of MIL-101b was attributed to its high adsorption heat (9.3 to 10.0 kJ mol^{-1} at low coverage), which was larger than that of MIL-100 (5.6 to 6.3 kJ mol^{-1} at low coverage). The nature of the interaction between hydrogen molecules and the framework that gave rise to such high values for MIL-101b is due to the presence of strong adsorption sites within the microporous supertetrahedra (ST), probably at each corner close to the trimers of chromium octahedra.[71]

2.5. Ni-Based MOFs

Lee and Suh reported a robust Ni-based metal–organic open framework, $[Ni(cyclam)(BPYDC)] \cdot 5H_2O$, which is constructed of linear coordination polymer chains made of the nickel–macrocyclic complex $[Ni(cyclam)](ClO_4)_2$ (cyclam = 1,4,8,11-tetraazacyclotetradecane) and 2,2′-bipyridyl-5,5′-dicarboxylate ($BPYDC^{2-}$).[72,73] This framework exhibits permanent microporosity with a Langmuir surface area of 817 m^2 g^{-1} and pore volume of 0.37 cm^3 cm^{-3}.[72] It adsorbed 1.1 wt% of hydrogen at 77 K and 1 bar. Forster et al. synthesized a Na/Ni-based framework $NaNi_3(OH)(SIP)_2$ (SIP = 5-sulfoisophthalate), consisting of $Na_2Ni_6O_{34}$ clusters bridged by SIP to form a 3D network.[74a] The dehydration of this framework at temperatures between 573 and 623 K generated a porous material with a BET surface area above 700 m^2 g^{-1}. Furthermore, the dehydrated framework possesses accessible, coordinatively unsaturated Ni^{II} sites, which leads to a high adsorption heat of 9.4–10.4 kJ mol^{-1}

for the hydrogen molecule. However, the H_2 capacity of this Ni-based framework at 1 bar and 77 K is only 0.94 wt% because of its medium surface area.

Dietzel et al. synthesized a Ni-based coordination polymer, $Ni(DHTP)(H_2O)_2 \cdot 8H_2O$ (DHTP = 2,5-dihydroxyterephthalic), which is a 3D honeycomb-like network with channels of ≈11 Å diameter and a Langmuir surface area of 1083 m^2 g^{-1}.[74] H_2 adsorption on the network at 77 K exhibited a type I profile, with which the Langmuir equation yields a saturation value of 1.8 wt% hydrogen capacity.

Zhao et al. evaluated three Ni-based MOFs (denoted as M, E, and C) for hydrogen adsorption and desorption. M and E have the composition $Ni_2(BPY)_3(NO_3)_4$ with linear chains of BPY bridging metal centers, which are connected by T-shaped BPY coordination at the metal into pairs. These pairs were aligned parallel to each other in M and perpendicular in E to form maximum pore cavity dimensions of 8.3 Å.[33] The cavities of MOFs M and E are connected by narrower windows, but the dynamics of the bridging BPY molecules confer sufficient flexibility on the framework to allow adsorptives (that appear oversized from a static view of the structure) to pass through the windows and access the pores.[75,76] C, with formula $Ni_3(BTC)_2(3\text{-}PIC)_6(PD)_3$ (where PIC = 3-picoline and PD = propane-1,2-diol), has considerably larger windows and cavities of up to 14 Å in size.[77] The adsorption–desorption isotherms for E and M showed a marked hysteresis, in which the former showed virtually no desorption even when the pressure was reduced from 1 to 0.01 bar.[33] In contrast, the adsorption–desorption isotherms of C did not show any substantial hysteresis up to 14 bar.[33] The maximum H_2 uptakes (at 77 K and 1 bar) on E, M, and C were 0.8, 0.7, and 2.1 wt%, respectively.[33] Notably, the hysteresis in H_2 uptake in porous MOF materials, in which the pore window dimensions are similar to the kinetic diameter of H_2, differs qualitatively from more rigid classical sorbents. Hydrogen can be loaded at high pressure and stored at low pressure, if the cavities are larger than the windows, which in turn are both close in size to H_2 and have sufficient flexibility due to framework dynamics to allow kinetic trapping of the guest molecule.[33] Therefore, the design of MOF materials with thermally activated windows in the open channel structure provides a new possibility to improve their hydrogen-storage characteristics by modifying the desorption kinetics.

2.6. Other MOFs

Perles et al. synthesized a 3D polymeric terephthalate of scandium $[Sc_2(C_8H_4O_4)_3]$ under hydrothermal conditions by the reaction of Sc^{3+} with a mixture of terephthalic acid and disodium terephthalate. The structure consists of a polymeric 3D framework, in which each scandium atom is octahedrically coordinated to six carboxylic oxygen atoms of six different terephthalate anions.[78] Such a structured $[Sc_2(C_8H_4O_4)_3]$ has a BET surface area of 721 m^2 g^{-1} and a micropore volume of 0.293 cm^3 g^{-1}.[78] It exhibited a hydrogen uptake of 1.5 wt% at 77 K and 0.8 bar.[78]

Kaye and Long examined hydrogen adsorption on dehydrated Prussian blue analogues of the type $M_3[Co(CN)_6]_2$ (M = Mn, Fe, Co, Ni, Cu, Zn), wherein interactions with bridging cyanide ligands and/or coordinatively unsaturated metal centers lead to higher adsorption heat.[79] They reported that the BET surface areas range from 560 m^2 g^{-1} for $Ni_3[Co(CN)_6]_2$ to 870 m^2 g^{-1} for $Mn_3[Co(CN)_6]_2$. The hydrogen uptake for the cyano-bridged frameworks varied from 1.4 wt% in $Zn_3[Co(CN)_6]_2$ to a maximum of 1.8 wt% in $Cu_3[Co(CN)_6]_2$ at 77 K and 1 bar. The heat of hydrogen adsorption is in a range of 5.9 kJ mol^{-1} for $Mn_3[Co(CN)_6]_2$ to 7.4 kJ mol^{-1} for $Ni_3[Co(CN)_6]_2$.[79]

Lee et al. synthesized a trinuclear $[Co_3(BPDC)_3BPY] \cdot 4DMF \cdot H_2O$ framework, which has a similar structure to $[Zn_3(BPDC)_3BPY] \cdot 4DMF \cdot H_2O$.[51] The hydrogen uptake of the $[Co_3(BPDC)_3BPY] \cdot 4DMF \cdot H_2O$ framework is 1.98 wt% at 77 K and 1 bar, which is higher than the 1.74 wt% of $[Zn_3(BPDC)_3BPY] \cdot 4DMF \cdot H_2O$. The difference in the H_2 uptake between the two frameworks can be attributed to their different surface areas (922 m^2 g^{-1} for the Co-based framework and 792 m^2 g^{-1} for the Zn-based framework), pore volumes (0.38 cm^3 g^{-1} for the former and 0.33 cm^3 g^{-1} for the later), and strengths of gas–solid interactions.[51]

Dincă and Long reported the synthesis of $Mg_3(NDC)_3(DEF)_4$ (NDC = 2,6-naphthalenedicarboxylate), which is the first porous MOF incorporating Mg^{2+}.[80] Its structure consists of linear Mg_3 units linked by NDC bridges to form a 3D framework, featuring 1D channels filled with DEF molecules. Such a 3D framework structure is fully analogous to that of $Zn_3(NDC)_3(CH_3OH)_2 \cdot 2DMF \cdot H_2O$, which indicates that Mg^{2+} can directly substitute for the heavier Zn^{2+}.[80] The desolvation of $Mg_3(NDC)_3(DEF)_4$ by heating at 190 °C generated the microporous solid $Mg_3(NDC)_3$. This microporous framework has a high H_2 adsorption heat (7.0–9.5 kJ mol^{-1}). However, it exhibited a small hydrogen uptake of 0.48 wt% at 77 K and 1 bar because of its small BET surface area (190 m^2 g^{-1}).[80]

3. Hydrogen Storage in MOFs at Ambient Temperature

As discussed in the above section, MOFs have a high hydrogen uptake (even higher than 7 wt%) at a temperature of 77 K. However, the hydrogen capacities of these MOFs are usually below 2 wt% at ambient temperature with acceptable pressures (Table 2).[24,32,41,54,66,71,81–83] Such a low hydrogen uptake at ambient temperature is due to a weak binding of H_2 to MOFs. According to Bathia and Myers,[84] a thermodynamic requirement for an adsorbent capable of storing hydrogen at ambient temperature is 15.1 kJ mol^{-1} of hydrogen-adsorption heat. However, the heat of hydrogen adsorption reported to date for the MOFs are usually in the range of 4–7 kJ mol^{-1} with the highest value of 7.0–12 kJ mol^{-1} at low surface coverage.[66,71] Several approaches have been employed or proposed to increase the interactions between hydrogen and MOFs.

3.1. Optimization of Cations

As shown in Table 2, Zn-based MOFs usually have poor performance for hydrogen adsorption because of their low

Table 2. Summary of hydrogen adsorption on MOFs at ambient temperature.

Materials [a]	Apparent surface area [b] [m^2 g^{-1}]	Heat of adsorption [kJ mol^{-1}]	H_2 uptake [wt%]	Conditions	Ref.
$Zn_4O(BDC)_3$, MOF-5 or IRMOF-1	/	/	0.01	RT, 67 bar	[54]
	/	/	0.2	RT, 67 bar	[54]
	/	/	0.1	RT, 10 bar	[54]
	/	/	0.5	RT, 10 bar	[24]
	/	/	0.23	RT, 10 bar	[41]
	/	/	0.4	RT, 100 bar	[96]
Pt/AC+MOF-5 mixture	/	/	1.6	RT, 100 bar	[96]
Pt/AC+MOF-5 with carbon bridges	/	/	3.0	RT, 100 bar	[96]
Li-decorated MOF-5	/	/	2.9 [f]	200 K, 1 bar	[88]
	/	/	2.0 [f]	300 K, 1 bar	[88]
$Zn_4O(R^6\text{-}BDC)_3$, IRMOF-6	2630	/	1.0	RT, 10 bar	[24,105]
$Zn_4O(NDC)_3$, IRMOF-8	/	/	2.0	RT, 10 bar	[24]
	/	/	0.5	RT, 100 bar	[96]
Pt/AC+IRMOF-8 mixture	/	/	1.8	RT, 100 bar	[96]
Pt/AC+IRMOF-8 with carbon bridges	/	/	4.0	RT, 100 bar	[96]
$Zn_4O(BTB)_2$, MOF-177	4300, 3100 [c]	−11.3/−5.8 [e]	0.62	RT, 100 bar	[82]
Pt/AC+MOF-177 mixture (spillover)	/	/	1.5	RT, 100 bar	[82]
$Zn_4O(L^1)_3$	502 [d]	/	1.12	RT, 48 bar	[32]
$Zn_4O(L^2)_3$	396 [d]	/	0.98	RT, 48 bar	[32]
Pt/C+MIL-53(Cr)	/	/	0.43	293 K, 50 bar	[83]
Pt/C+MIL-53 with carbon bridges	/	/	0.63	293 K, 50 bar	[83]
MIL-101	/	/	0.37	293 K, 50 bar	[83]
Pt/C+MIL-101	/	/	0.75	293 K, 50 bar	[83]
Pt/C+MIL-101with carbon bridges	/	/	1.14	293 K, 50 bar	[83]
$Cu_2(HFIPBB)_2(H_2HFIPBB)$	/	/	1.0	RT, 48 bar	[41]
MOF-C30	/	/	0.25 [f]	RT, 20 bar	[81]
	/	/	0.56 [f]	RT, 50 bar	[81]
Li-MOF-C30	/	/	3.89[f]	RT, 20 bar	[81]
	/	/	4.56 [f]	RT, 50 bar	[81]
	/	/	5.16 [f]	RT, 100 bar	[81]
$Li_6\text{-}C_{20}H_{10}$	/	/	4.58 [f]	300 K, 230 bar	[91]
	/	/	6.5	300 K, 215 bar	[91]
$[Mn(DMF)_6]_3[(Mn_4Cl)_3(BTT)_8(H_2O)_{12}]_2 \cdot 42CH_3OH$	/	/	1.5	298 K, 90 bar	[66]
$COF(BTC)_2$, MIL-100(Cr)	/	/	0.15	RT, 73 bar	[71]
$Cr_3OF(BDC)_3$, MIL-101(Cr)	/	/	0.43	RT, 80 bar	[71]

[a] Acronyms: BDC = benzene-1,4-dicarboxylate; R^6-BDC = 1,2-dihydrocyclobutylbenzene-3,6-dicarboxylate, NDC = naphthalene-2,6-dicarboxylate; BTB = benzene-1,3,5-tribenzoate; L^1 = 6,6′-dichloro-2,2′-diethoxy-1,1′-binaphthyl-4,4′-dibenzoate; L^2 = 6,6′-dichloro-2,2′-dibenzyloxy-1,1′-binaphthyl-4,4′-dibenzoate; HFIPBB = 4,4′ (hexafluoroisopropylidene)-bis(benzoate); H_2HFIPBB = 4,4′-(hexafluoroisopropylidene)-bis(benzoic acid); BTT = 1,3,5-benzenetristetrazolate; BTC = benzene-1,3,5-tricarboxylate. [b] Calculated from N_2 adsorption at 77 K using the Langmuir model except where indicated. [c] BET surface area from N_2 adsorption at 77 K. [d] BET surface area from CO_2 adsorption at 273 K. [e] Values obtained from adsorption experiments at different temperatures. [f] Values deduced from simulations.

binding energy with H_2.[24,32,41,54,66,71,83,85] Searching effective metals for MOFs is a high priority for synthetic chemists. So far, the Mn-based and Cr-based MOFs exhibit the high heats (10 kJ mol^{-1}) of H_2 molecule adsorption.[66,71] Even these high heats are still much lower than 15.1 kJ mol^{-1}, resulting in only about 0.43wt% H_2 uptake (for Cr-based MOF)[71] and 1.5 wt% uptake (for Mn-based MOF)[66] at ambient temperature and a pressure of about 80 bar. However, from the density functional theory (DFT)-Perdew–Burke–Erznerhof (PBE) calculations,[86] Sun et al. found that the binding energy to H_2 can be tuned from about 10 to 50 kJ mol^{-1} by using different transition metals in the MOF systems. The binding energies to hydrogen molecules were 10.4, 21.9, 34.6, and 46.5 kJ mol^{-1} for Mn, Sc, Ti, and V in MOFs, respectively. However, because calculation results are strongly dependent on calculation approaches and selected models, it would be important to verify those theoretical predictions by experimental measurements.

3.2. Doping Li into MOFs

Recently, the effect of Li on properties of MOFs was explored by several theoretic research groups.[81,87–91] The following theoretical predictions for the effect of Li on hydrogen in MOFs at room temperature are very promising. However, no experimental data are yet available in the literature to support these predictions.

Han and Goddard's grand canonical ensemble Monte Carlo (GCMC) simulations demonstrated that doping of MOFs with Li is an effective way to increase the binding of H_2 to MOFs.[81] Their GCMC simulations were based on the first-principles-derived force field (FF). This FF-based GCMC technique was validated by the fact that the results obtained from the FF-GCMC simulations were in a good agreement with experimental data for H_2 adsorption on MOFs without Li. Han and Goddard employed this novel technique to simulate five Li-doped MOFs (Fig. 8). They

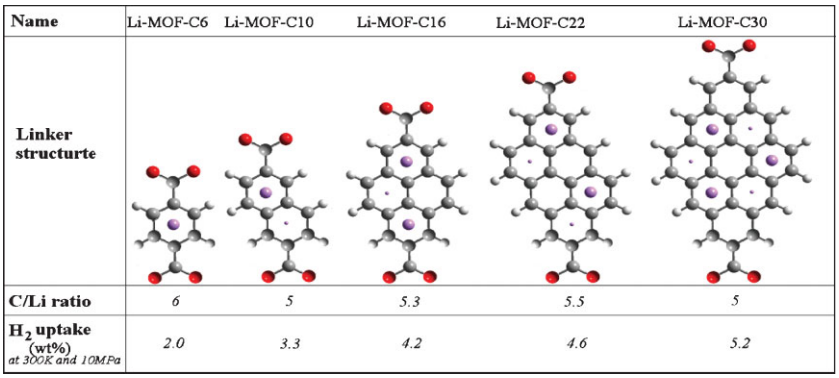

Figure 8. Li-doped MOFs. In each framework, the $Zn_4O(CO_2)_6$ connector couples to six aromatic linkers through the O–C–O common to each linker. The large and small violet atoms in the linkers represent Li atoms above and below the linkers, respectively. Reproduced with permission from ref. [81]. Copyright 2007, American Chemical Society.

found that Li atoms preferred to bind at centers of the hexagonal aromatic rings, but Li atoms on adjacent aromatic rings were on opposite sides. Furthermore, their results showed that at 300 K, Li-MOF-C30 (molar ratio of C to Li is 5) had 3.89 wt% H_2 uptake at 20 bar and 4.56 wt% uptake at 50 bar, which is the highest reversible hydrogen-storage capacity at room temperature yet reported. In contrast, the corresponding hydrogen uptakes of pure MOF-C30 were only 0.25 and 0.56 wt% at 20 and 50 bar, respectively. This indicated that doping of MOFs with Li can increase hydrogen uptake at ambient temperature by almost 10 times. Furthermore, when the pressure of hydrogen went up to 100 bar, Li-MOF-C30 could store 5.16 wt% of H_2 at 300 K, 5.57 wt% at 273 K, and 5.99 wt% at 243 K, reaching the DOE 2010 targets of 6 wt% at a temperature between 243 and 353 K (−30 and 80 °C). The presence of Li is the critical factor for high H_2 uptake at ambient temperature. For the MOFs without Li, the H_2 molecule bound weakly to both the metal oxide clusters and the aromatic linkers, resulting in small binding energies of 6.3 and 3.8 kJ mol^{-1}, respectively. As a result, remarkable H_2 uptake in pure MOF systems can be obtained only at a temperature of 77 K or below. In contrast, for the Li-MOFs, the high electron affinity of the aromatic sp^2 carbon framework can create the positive Li sites, leading to a strong stabilization of molecular H_2. Indeed, Li-doped MOFs exhibited high binding energies of 16.7 kJ mol^{-1} with H_2, which results in a high H_2 uptake at ambient temperature. Such a strong interaction between H_2 and Li-doped MOFs was supported by the DFT calculations and GCMC simulations from other groups.[87,88] However, Blomqvist et al. found that, although each Li on the organic linkers is able to bind up to three H_2 molecules, only two hydrogen molecules can successfully coordinate to each Li because of dynamical effects that prevent the third H_2 molecule from being adsorbed.[88] In other words, the dynamical effects may decrease the hydrogen capacity on Li-doped MOFs.

Although the above theoretical predictions have not yet been examined experimentally, the promoting effect of Li^+ on H_2 adsorption on a twofold interwoven MOF was confirmed by Mulfort and Hupp.[92,93] They carried out experimental measurements for H_2 adsorption on $Zn_2(NDC)_2(diPyNI)$ (NDC = 2,6-naphthalenedicarboxylate; diPyNI = N,N′-di-(4-pyridyl)-1,4,5,8- naphthalenetetracarboxydiimide) with and without Li^+ doping at 77 K.[92,93] Their results showed that the H_2 capacity of $Zn_2(NDC)_2(diPyNI)$ was 0.93 wt% at 77 K and 1 bar, but Li^+-doped $Zn_2(NDC)_2$ (diPyNI) had nearly double the H_2 capacity(1.63 wt%). A similar effect of Li on hydrogen storage in MIL-53(Al) was also observed.[94] The adsorption capacity of hydrogen was 1.7 and 0.5 wt% at 77 K and 1 bar for MIL-53(Al) samples with and without Li, respectively.[94] This indicates that the hydrogen uptake of Li-doped MIL-53(Al) is larger than that of pure MIL-53(Al). However, these results were obtained at a very low temperature of 77 K and a low pressure of 1 bar. The effect of Li on hydrogen storage in MOFs is still waiting for experimental confirmation at ambient temperature and high pressure.

3.3. Doping MOFs with Catalysts

Breakthrough research has been done by Li and Yang.[95] They developed a novel approach that can markedly enhance hydrogen capacities by doping Pt/AC (activated-carbon) catalysts into MOFs. At 298 K and 100 bar, 1.6 wt% reversible hydrogen capacity can be reached on the mechanical mixture of Pt/AC and MOF-5 and 1.8 wt% on the mechanical mixture of Pt/AC and IRMOF-8,[96] which were much higher than those without the Pt/AC catalyst (only about 0.4 wt%). The enhancement was attributed to atomic hydrogen spillover on carbon and secondary spillover on MOFs, that is, hydrogen molecules were dissociated into hydrogen atoms on Pt catalytic sites, followed by diffusion to the carbon surface and then to the MOF surface. Furthermore, the reversible hydrogen capacity can reach even 4 wt% at 298 K and 100 bar, if Pt/AC and IRMOF-8 were well-connected by more carbon bridges generated by sucrose carbonization (Fig. 9).[96] This is the highest experimental capacity of hydrogen yet reported for MOFs at ambient temperature. Furthermore, no apparent saturation value was approached for the sample as the isotherm was linear even at 100 bar. The absence of a saturation value suggests a further increase in capacity at higher pressures. The hydrogen uptake of 6 wt% was predicted at 298 K and 150 bar. Such high hydrogen uptakes can be attributed to their high adsorption heats that ranged between 20 and 23 kJ mol^{-1}, which are higher than 15.1 kJ mol^{-1}.[96] This occurred because atomic hydrogen has a much stronger binding ability to both metal oxides and organic linkers than molecular hydrogen. They obtained similar results by using the combination of a Pt/AC catalyst with other MOFs (MOF-177, COF-1, HKUST-1, or MIL-101) via carbon bridges.[97,82] A comparison of these combinations indicated that the surface area and pore volume of the material were not the predominant factors that determined the hydrogen adsorption capacity by atomic hydrogen spillover.[97,82] However, a correlation between the hydrogen uptake by the spillover and the heat of adsorption of the material was

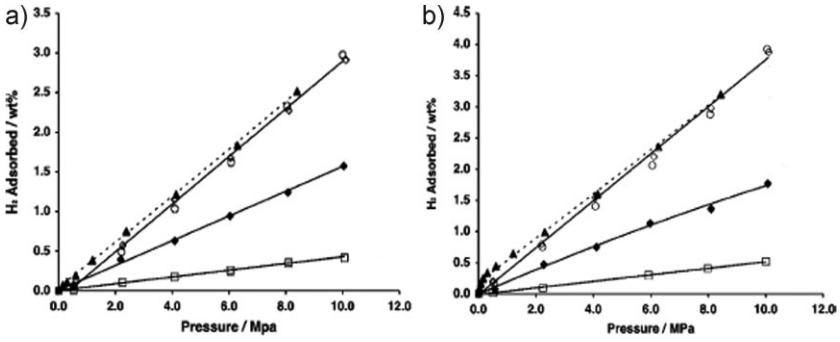

Figure 9. High-pressure hydrogen isotherms at 298 K. a) Pure IRMOF-1 (□), Pt/AC and IRMOF-1 physical mixture (1:9 weight ratio) (◆), and for a bridged sample of Pt/AC-bridges–IRMOF-1: first adsorption (○), desorption (▲), and second adsorption (◇). b) Pure IRMOF-8 (□), Pt/AC and IRMOF-8 physical mixture (1:9 weight ratio) (◆), and for a bridged sample of Pt/AC-bridges–IRMOF-8: first adsorption (○), desorption (▲), and second adsorption (◇). Reproduced with permission from ref. [96]. Copyright 2006, American Chemical Society.

found, which indicates the importance of the strength of the interaction between atomic hydrogen and MOFs in hydrogen adsorption at ambient temperature. Such interesting results are attracting attention from other researchers.[83,98]

4. Effects of Surface Areas and Pore Sizes on Hydrogen Storage in MOFs

Surface area plays an important role in gas adsorption on solid materials. As a general principle, the maximum (saturated) adsorbed amount of gas on a solid surface is dependent on its surface area. This was well-demonstrated by correlating the hydrogen-storage capacity with specific surface area for zeolites and carbon materials at a low temperature, such as 77 K.[99] However, when the pressure of the gas is not high enough to reach its saturated adsorption, the amount of the adsorbed gas is mainly determined by the interaction between the gas and the solid surface (reflected by adsorption heat).[26] This can explain why no correlation exists between hydrogen-storage capacity and the specific surface area of MOFs at a pressure of 1 bar or below, which is much lower than that required for the saturated adsorption on the MOFs.[37] In contrast, the saturated hydrogen capacity, which corresponds to the plateau of the adsorption isotherm at 77 K, correlates almost linearly to the specific surface area for the MOFs.[35,100] Nevertheless, it should be noted that there are some exceptions for H_2 storage in MOFs. For example, although the BET surface area (5500 m^2 g^{-1}) of MIL-101b (Cr-based MOF) is higher than that (4746 m^2 g^{-1}) of MOF-177 (Zn-based MOF), its saturated H_2 capacity (6.1 wt%) is lower than that (7.5 wt%) of MOF-177 at 77 K.[35,71] These exceptions might be a result of inappropriate measurement of surface areas. The BET equation is applicable to materials with large pores (e.g., mesoporous materials) in the absence of capillary condensation, but is not strictly suitable to microporous materials, such as MOFs.

Pore size can affect the interaction between hydrogen molecules and porous solids, namely materials that contain small pores with walls of high curvature interact with hydrogen molecules more strongly than large-pore materials.[28a,27] The ideal pore size might be slightly larger than the kinetic diameter of H_2 (2.8 Å) for low-pressure adsorption, because pores with such a small size allow the dihydrogen molecule to interact with multiple portions of the framework rather than just one SBU or organic linker, which increases the interaction energy between the framework and H_2.[27] Furthermore, Panella et al. obtained a linear relationship between hydrogen-desorption temperature and pore sizes of MOFs, which indicates that a MOF with smaller pores requires a higher desorption temperature than a larger-pore MOF (Fig. 10).[100] This provides solid evidence that the smaller the pores, the stronger the adsorption of H_2.

5. Mechanism of Hydrogen Adsorption on MOFs

In order to enhance the ability of hydrogen storage, MOF materials would require optimizing the attractive intermolecular interactions between the hydrogen and the condensed phase environment. In principle, there are two main types of sites for hydrogen adsorption: one associated with inorganic metal clusters and another associated with organic linkers. Several research groups evaluated the interaction of hydrogen molecules with the metal oxide sites and organic linker sites.[101–105] The neutron powder diffraction along with first-principle calculations showed that the metal–oxide cluster was primarily responsible for hydrogen adsorption, while the organic linker played only a secondary role.[101,106,107] Furthermore, the neutron-diffraction

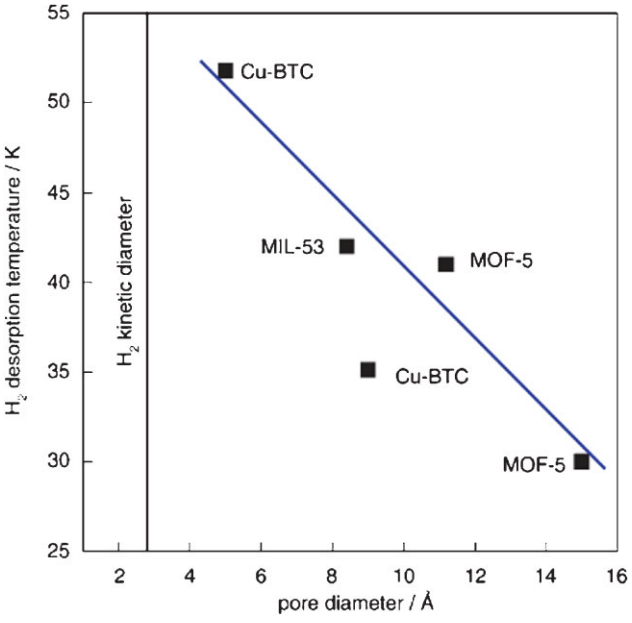

Figure 10. Thermal desorption temperatures of hydrogen in MOFs versus the diameter of their pores. Reproduced from ref. [100].

analysis at 3.5 K on deuterated MOF-5 revealed four sites for adsorption of hydrogen molecules.[95,102] The two sites were found to be filled first: one at the center of the three ZnO_3 triangular faces and one on top of the single ZnO_3 triangle. On further loading, two additional adsorption sites were occupied: one above the two oxygen ions and one at the top of the hexagonal linkers. The relative binding energies were found to be larger for the three sites around the clusters than for the one site around the organic linkers.[101,108] This was supported by the high-quality second-order Moller–Plesset (MP2) calculations.[109] The MP2 calculations showed that the binding energy of H_2 on the zinc oxide corners using $Zn_4O(HCO_2)_6$ molecule as a model was 6.28 kJ mol^{-1},[109] whereas the binding energies of H_2 to the organic linkers were 4.16–5.42 kJ mol^{-1} depending on the size of the linkers.

The molecular simulation showed that, although the metal–oxygen clusters were preferential adsorption sites for hydrogen in MOFs, the effect of the organic linkers became evident with increasing pressure.[110] This is because the sites on the organic linker have lower binding energies but a much greater capacity for increases in H_2 loading.[103,106] Binding of H_2 at the inorganic cluster sites was also affected by the nature of the organic linker.[103] Furthermore, the DFT calculations showed that the larger the linker, the stronger the binding between H_2 and the linker.[111]

Properties of the interactions between H_2 and MOFs were evaluated. Bordiga et al. reported that the adsorptive properties of MOF-5 were mainly a result of the weak electrostatic forces associated with $O_{13}Zn_4$ clusters and the dispersive interactions with the internal wall structure.[102] Recently, Belof et al. employed Monte Carlo simulations to model hydrogen sorption in *soc*-MOF, $[In_3O(C_{16}N_2O_8H_6)_{1.5}]NO_3$.[112] Unlike most other MOFs that have been investigated for hydrogen storage, *soc*-MOF had a highly ionic framework and many relatively small channels (around 1 nm in diameter).[112] The simulations demonstrated that, for a high hydrogen capacity, MOFs should have relatively small pores and interconnected pores with a high surface area to create strong MOF–H_2 interactions and, thus, indirectly H_2–H_2 attractions. To promote these interactions, the MOF also needs to be locally polar with large charge separations on its surface sufficiently far apart to allow hydrogen molecules to be sensitive to the dipolar interface. Microscopically, hydrogen interacts with the MOF by three principle attractive potential energy contributions: Van der Waals, charge–quadrupole, and induction.[112] The polarization interactions strongly influence the structure of the adsorbed hydrogen in the region of the metal ions and lead to two distinct populations of dipolar hydrogen.[112] The cooperative interactions may also play an important role. Lee et al. revealed that hydrogen adsorption occurred by a cooperative mechanism in which the adsorptions on metal sites initiated the propagation of the adsorption across the whole framework.[113] The simultaneous adsorption of two hydrogen molecules was more favorable than individual adsorption of two hydrogen molecules, which indicated that adsorbed hydrogen molecules have a remarkable interaction.[113] Furthermore, the DFT-PBE calculations revealed an important role of the orbital interactions between a transition metal (TM) in MOFs and H_2 for hydrogen adsorption [86].

The diffusion of H_2 in MOFs was first investigated by Skoulidas and Sholl.[114] They employed equilibrium molecular dynamics to probe the self- and transport-diffusivities of H_2 in MOF-5 at room temperature. This work was followed by the studies of Yang and Zhong[110] and Liu et al.[115] Yang and Zhong performed a systematic molecular simulation to evaluate the self-diffusivities of H_2 in MOF-5, IR-MOF-8, and IRMOF-18 at 77 K.[110] They found that the self-diffusivities of H_2 in these MOFs are the same order of magnitude as diffusion of H_2 in some zeolites. However, from the neutron scattering measurements, Salles et al. found that the diffusivity of hydrogen at low loading is about 100 times higher in MIL-47(V) and MIL-53(Cr) frameworks than in zeoiltes.[116] Furthermore, MIL-47(V) exhibited a significantly higher diffusivity than MIL-53(Cr) because of the presence of μ_2-OH groups in MIL-53(Cr). The μ_2-OH groups could act as attractive sites and steric barriers for H_2, which results in a resistance to H_2 diffusion. Furthermore, in H_2 and D_2 adsorption and desorption kinetics experiments, Chen et al. observed quantum effects on hydrogen diffusion in a mixed zinc/copper MOF $Zn_3(BDC)_3[Cu(PYEN)] \cdot (DMF)_5 \cdot (H_2O)_5$, namely, 1D diffusion in very narrow porosity in the *b*-axis direction was a slow process.[64] These results indicate that the nature of the skeleton of the MOFs strongly affects H_2 diffusion.

6. Techniques for Hydrogen Capacity Measurements

It is important to accurately determine the H_2 capacity during H_2 adsorption and desorption. One of the conventional methods is thermogravimetry, which determines the H_2 capacity by the weight change. The major disadvantage of thermogravimetry is that any H_2O impurity can lead to a significant error. This happens because the weight of a H_2O molecule is equal to the weight of nine H_2 molecules. Even though the concentration of the H_2O impurity in H_2 is as low as several ppm, the sample is usually kept in a H_2 flow for a certain time to determine the weight change. As a result, the sample can adsorb a significant amount of H_2O, particularly in small samples and during prolonged measurements. For example, 0.5 wt% of H_2O adsorbed can be thought as 4.5 wt% of H_2 capacity. In contrast, the volumetric method determines the pressure change of H_2 during adsorption (or desorption) in a closed chamber. As a result, the adsorption of H_2O can lead to a much lower error in the hydrogen capacity in the volumetric method. For this reason, most hydrogen capacities discussed above were obtained by using volumetric method.[35–37,51,54,65–67,71,72,74b,78–80,92,93,95,96] Furthermore, these hydrogen capacities were calculated on the material basis. However, for a practical hydrogen-storage system, hydrogen capacities should be calculated on the system basis, including storage materials and tank.

7. Outlook

MOFs exhibit excellent performance for hydrogen adsorption at 77K. However, it is still a challenge for MOFs to store hydrogen at ambient temperature. This is because the interaction between molecular hydrogen and MOFs is relatively weak. Bhatia and Myers obtained the thermodynamic requirement for an adsorbent capable of storing hydrogen at ambient temperature,

which is a heat of adsorption of hydrogen equal to 15.1 kJ mol^{-1}.[84] This value is optimal with respect to the affinity of hydrogen, which is strong enough to store a large amount of hydrogen gas at the charging pressure (about 30 bar) but weak enough to release most of that hydrogen at the discharge pressure (about 1.5 bar). Furthermore, Frost et al. reported similar requirements for hydrogen adsorption heat with a consideration about the effect of free volume.[117] These requirements can be used as criteria to search and design MOFs for hydrogen storage at ambient temperature. However, so far, there is no material to reach those criteria by molecular hydrogen adsorption.

Searching suitable metals and modifying organic linkers are still important approaches to explore MOFs. DFT-PBE calculations have demonstrated that the binding energies to hydrogen molecules were 21.9, 34.6, and 46.5 kJ mol^{-1} for Sc, Ti, and V in MOFs, respectively.[86] This provides a helpful guide for experimental researchers to design and synthesize effective MOFs that will have a larger heat of hydrogen adsorption than 15.1 kJ mol^{-1}.

Doping MOFs by Li or other electropositive metals should be another promising strategy to increase hydrogen capacity at ambient temperature, because it was theoretically predicted that the reversible hydrogen capacity of Li-doped MOFs at ambient temperature and 150 bar can reach 6 wt%.[81]

So far, promising results at ambient temperature were obtained with a Pt/AC catalyst-promoted IRMOF-8 material, which displayed 4 wt% hydrogen uptake at 100 bar with a prediction of 6 wt% at 150 bar.[95,96] This indicates that doping MOFs by catalysts is an effective approach to increase hydrogen capacity at ambient temperature. This occurred because hydrogen adsorption on metal-catalyst-promoted MOFs took place by atomic hydrogen instead of molecular hydrogen, which results in a high adsorption heat (above 20 kJ mol^{-1}). Although MOF-5 has almost double the surface area of IRMOF-8, its hydrogen uptake was lower than that of IRMOF-8 when they were combined with a Pt/AC catalyst.[95,96] This indicates that the hydrogen uptake by atomic hydrogen adsorption at ambient temperature is strongly dependent on the organic linkers of MOFs. For this reason, it can be expected that higher hydrogen uptakes can be obtained by applying Pt/AC catalysts to other MOFs. Furthermore, it is also worthwhile to explore other catalysts for combination with MOFs.

Acknowledgements

This work is supported by the USA NSF (CBET- 0929207).

Received: June 22, 2009
Published online:

[1] L. Schlapbach, A. Züttel, *Nature* **2001**, *414*, 353.
[2] M. Fichtner, *Adv. Eng. Mater.* **2005**, *7*, 443.
[3] S. I. Orimo, Y. Nakamori, J. R. Eliseo, A. Zuttel, C. M. Jensen, *Chem. Rev.* **2007**, *107*, 4111.
[4] B. Bogdanovic, M. Schwichardi, *J. Alloys Comp.* **1997**, *253*, 1.
[5] C. M. Jensen, K. J. Gross, *J. Appl. Phys. A.* **2001**, *72*, 213.
[6] a) Y. H. Hu, E. Ruckenstein, *J. Phys. Chem. A* **2003**, *107*, 9737. b) Y. H. Hu, E. Ruckenstein, *Ind. Eng. Chem. Res.* **2006**, *45*, 4993. c) Y. H. Hu, E. Ruckenstein, *Ind. Eng. Chem. Res.* **2004**, *43*, 2464.
[7] G. Sandrock, in *Handbook of Fuel Cells*, (Eds: W. Vielstich, A. Lamm, H. A. Gasteiger,) Wiley, New York **2003**, p. 101.
[8] A. M. Seayad, D. M. Antonelli, *Adv. Mater.* **2004**, *16*, 765.
[9] W. Grochala, P. P. Edwards, *Chem. Rev.* **2004**, *104*, 1283.
[10] W. L. Mao, H. K. Mao, A. F. Goncharov, V. V. Struzhkin, Q. Guo, J. Hu, J. Shu, R. J. Hemley, M. Somayazulu, Y. Zhao, *Science* **2002**, *297*, 2247.
[11] Y. H. Hu, E. Ruckenstein, *Angew. Chem. Int. Ed.* **2006**, *45*, 2011.
[12] C. O. Arean, *J. Phys. Chem. B* **2006**, *110*, 395.
[13] R. Strobel, J. Garche, P. T. Moseley, L. Jorissen, G. Wolf, *J. Power Sources* **2006**, *159*, 781.
[14] D. Golberg, Y. Bando, C. C. Tang, C. Y. Zhi, *Adv. Mater.* **2007**, *19*, 2413.
[15] D. Maspoch, D. Ruiz-Molina, J. Veciana, *Chem. Soc. Rev.* **2007**, *36*, 770.
[16] B. F. Hoskins, R. Robson, *J. Am. Chem. Soc.* **1989**, *111*, 5962.
[17] B. F. Abrahams, B. F. Hoskins, J. Liu, R. Robson, *J. Am. Chem. Soc.* **1991**, *113*, 3045.
[18] O. Yaghi, G. M. Li, H. L. Li, *Nature* **1995**, *378*, 703.
[19] M. Fujita, D. Oguro, M. Miyazawa, H. Oka, K. Yamaguchi, K. Ogura, *Nature* **1995**, *378*, 469.
[20] J. S. Seo, D. Whang, H. Lee, S. I. Jun, J. Oh, Y. J. Yeon, K. Kim, *Nature* **2000**, *404*, 982.
[21] G. Férey, *Chem. Soc. Rev.* **2008**, *37*, 191.
[22] S. I. Noro, S. Kitagawa, M. Kondo, K. Seki, *Angew. Chem. Int. Ed.* **2000**, *39*, 2091.
[23] M. Kondo, T. Yoshitomi, K. Seki, H. Matsuzaka, S. Kitagawa, *Angew. Chem. Int. Ed.* **1997**, *36*, 1725.
[24] N. L. Rosi, J. Eckert, M. Eddaoudi, D. T. Vodak, J. Kim, M. O'Keeffe, O. M. Yaghi, *Science* **2003**, *300*, 1127.
[25] J. L. C. Rowsell, O. M. Yaghi, *Angew. Chem. Int. Ed.* **2005**, *44*, 4670.
[26] M. Hirscher, B. Pabella, *Scripta Materialia* **2007**, *56*, 809.
[27] D. J. Collins, H. Zhou, *J. Mater. Chem.* **2007**, *17*, 3154.
[28] a) R. E. Morris, P. S. Wheatley, *Angew. Chem. Int. Ed.* **2008**, *47*, 4966. b) X. Lin, J. Jia, P. Hubberstey, M. Schroder, N. R. Champness, *Cryst. Eng. Commun.* **2007**, *9*, 438.
[29] M. Dincă, J. R. Long, *Angew. Chem. Int. Ed.* **2008**, *47*, 6766.
[30] K. M. Thomas, *Dalton Trans.* **2009**, 1487.
[31] D. N. Dybtsev, H. Chun, S. H. Yoon, D. Kim, K. Kim, *J. Am. Chem. Soc.* **2004**, *126*, 32.
[32] B. Kesanli, Y. Cui, M. R. Smith, E. W. Bittner, B. C. Bockrath, W. Lin, *Angew. Chem. Int. Ed.* **2005**, *44*, 72.
[33] X. B. Zhao, B. Xiao, A. J. Fletcher, K. M. Thomas, D. Bradshaw, M. J. Rosseinsky, *Science* **2004**, *306*, 1012.
[34] L. Pan, B. Parker, X. Y. Huang, D. H. Olson, J. Y. Lee, J. Li, *J. Am. Chem. Soc.* **2006**, *128*, 4180.
[35] A. G. Wong-Foy, A. J. Matzger, O. M. Yaghi, *J. Am. Chem. Soc.* **2006**, *128*, 3494.
[36] S. S. Kaye, A. Dailly, O. M. Yaghi, J. R. Long, *J. Am. Chem. Soc.* **2007**, *129*, 14176.
[37] J. L. C. Rowsell, A. R. Millward, K. S. Park, O. M. Yaghi, *J. Am. Chem. Soc.* **2004**, *126*, 5666.
[38] J. L. Rowsell, O. M. Yaghi, *J. Am. Chem. Soc.* **2006**, *128*, 1304.
[39] B. Panella, M. Hirscher, H. Pütter, U. Müller, *Adv. Funct. Mater.* **2006**, *16*, 520.
[40] A. Dailly, J. J. Vajo, C. C. Ahn, *J. Phys. Chem. B.* **2006**, *110*, 1099.
[41] L. Pan, M. B. Sander, X. Huang, J. Li, M. Smith, E. Bittner, B. Bockrath, J. K. Johnson, *J. Am. Chem. Soc.* **2004**, *126*, 1308.
[42] B. Panella, M. Hirscher, *Adv. Mater.* **2005**, *17*, 538.
[43] J. Hafizovic, M. Bjorgen, Unni Olsbye, P. D. C. Dietzel, S. Bordiga, C. Prestipino, C. Lamberti, K. P. Lillerud, *J. Am. Chem. Soc.* **2007**, *129*, 3612.
[44] M. Sabo, A. Henschel, H. Fröde, E. Klemm, S. Kaskel, *J. Mater. Chem.* **2007**, *17*, 3827.
[45] B. Chen, M. Eddaoudi, S. T. Hyde, M. O'Keeffe, O. M. Yaghi, *Science* **2001**, *291*, 1021.
[46] S. R. Batten, R. Robson, *Angew. Chem, Int. Ed.* **1998**, *37*, 1460.

[47] D. N. Dybtsev, H. Chun, K. Kim, *Angew. Chem. Int. Ed.* **2004**, *43*, 5033.
[48] J. Y. Lee, D. H. Olson, L. Pan, T. J. Emge, J. Li, *Adv. Funct. Mater.* **2007**, *17*, 1255.
[49] E. Y. Lee, S. Y. Jang, M. P. Suh, *J. Am. Chem. Soc.* **2005**, *127*, 6374.
[50] H. Chun, D. N. Dybtsev, H. Kim, K. Kim, *Chem. Eur. J.* **2005**, *11*, 3521.
[51] J. Y. Lee, L. Pan, S. R. Kelly, J. Jagiello, T. J. Emge, J. Li, *Adv. Mater.* **2005**, *17*, 2703.
[52] S. S. Y. Chui, S. M. F. Lo, J. P. H. Charmant, A. G. Orpen, I. D. Williams, *Science* **1999**, *283*, 1148.
[53] B. Chen, N. W. Ockwig, A. R. Millward, D. S. Contreras, O. M. Yaghi, *Angew. Chem. Int. Ed.* **2005**, *44*, 4745.
[54] X. Lin, J. Jia, X. Zhao, K. M. Thomas, A. J. Blake, G. S. Walker, N. R. Champness, P. Hubberstey, M. Schröder, *Angew. Chem. Int. Ed.* **2006**, *45*, 7358.
[55] S. A. Bourne, J. Lu, A. Mondal, B. Moulton, M. Zaworotko, *Angew. Chem. Int. Ed.* **2001**, *40*, 2111.
[56] B. Xiao, P. S. Wheatley, X. Zhao, A. J. Fletcher, S. Fox, A. G. Ross, I. L. Megson, S. Bordiga, L. Regli, K. M. Thomas, R. E. Morris, *J. Am. Chem. Soc.* **2007**, *129*, 1203.
[57] M. Dincă, A. F. Yu, J. R. Long, *J. Am. Chem. Soc.* **2006**, *128*, 8904.
[58] D. F. Sun, S. Q. Ma, Y. X. Ke, D. J. Collins, H. C. Zhou, *J. Am. Chem. Soc.* **2006**, *128*, 3896.
[59] P. Krawiec, M. Kramer, M. Sabo, R. Kunschke, H. Frode, S. Kaskel, *Adv. Eng. Mater.* **2006**, *8*, 293.
[60] K. Schlichte, T. Kratzke, S. Kaskel, *Micropor. Mesopor. Mater.* **2004**, *73*, 81.
[61] P. Küsgens, M. Rose, I. Senkovska, H. Fröde, A. Henschel, S. Siegle, *Micropor. Mesopor. Mater.* **2009**, *120*, 325.
[62] H. Frost, T. Duren, R. Q. Snurr, *J. Phys. Chem. B* **2006**, *110*, 9565.
[63] J. C. Liu, J. T. Culp, S. Natesakhawat, B. C. Bockrath, B. Zande, S. G. Sankar, G. Garberoglio, J. K. Johnson, *J. Phys. Chem. C* **2007**, *111*, 9305.
[64] B. Chen, X. Zhao, A. Putkham, K. Hong, E. B. Lobkovsky, E. J. Hurtado, A. J. Fletcher, K. M. Thomas, *J. Am. Chem. Soc.* **2008**, *130*, 6411.
[65] H. R. Moon, N. Kobayashi, M. P. Suh, *Inorg. Chem.* **2006**, *45*, 8672.
[66] M. Dincă, A. Dailly, Y. Liu, C. M. Brown, D. A. Neumann, J. R. Long, *J. Am. Chem. Soc.* **2006**, *128*, 16876.
[67] G. Férey, M. Latroche, C. Serre, F. Millange, T. Loiseau, A. Percheron-Guegan, *Chem. Commun.* **2003**, *24*, 2976.
[68] S. Surblé, C. Serre, F. Millange, T. DIren, M. Latroche, G. Férey, *J. Am. Chem. Soc.* **2006**, *128*, 14889.
[69] T. Loiseau, L. Lecroq, C. Volkringer, J. Marrot, G. Férey, M. Haouas, F. Taulelle, S. Bourrelly, P. L. Llewellyn, M. Latroche, *J. Am. Chem. Soc.* **2006**, *128*, 10223.
[70] T. Loiseau, C. Serre, C. Huguenard, G. Fink, G. Taulelle, M. Henry, T. Bataille, G. Férey, *Chem. Eur. J.* **2004**, *10*, 1373.
[71] M. Latroche, S. Surble, C. Serre, C. Mellot-Draznieks, P. L. Llewellyn, J. H. Lee, J. S. Chang, S. H. Jhung, C. Férey, *Angew. Chem. Int. Ed.* **2006**, *45*, 8227.
[72] E. Y. Lee, M. P. Suh, *Angew. Chem. Int. Ed.* **2004**, *43*, 2798.
[73] K. S. W. Sing, S. J. Greg, *Adsorption, Surface Area and Porosity*, 2nd ed. Academic Press, London **1982**, Ch. 1–5.
[74] a) P. M. Forster, J. Eckert, B. D. Heiken, J. B. Parize, J. W. Yoon, S. H. Jhung, J. S. Chang, A. K. Cheetham, *J. Am. Chem. Soc.* **2006**, *128*, 16 846. b) P. D. C. Dietzel, B. Blom, H. Fjellvag, *Chem. Commun.* **2006**, 959.
[75] A. J. Fletcher, E. J. Cussen, C. J. Kepert, M. J. Rosseinsky, K. M. Thomas, *J. Am. Chem. Soc.* **2003**, *123*, 10001.
[76] E. J. Cussen, J. B. Claridge, M. J. Rosseinsky, C. J. Kepert, *J. Am. Chem. Soc.* **2002**, *124*, 9574.
[77] D. Bradshaw, T. J. Prior, E. J. Cussen, J. B. Claridge, M. J. Rosseinsky, *J. Am. Chem. Soc.* **2004**, *126*, 6106.
[78] J. Perles, M. Iglesias, M. A. Martin-Luengo, M. A. Monse, C. Ruiz-Valero, N. Snejko, *Chem. Mater.* **2005**, *17*, 5837.
[79] S. S. Kaye, J. R. Long, *J. Am. Chem. Soc.* **2005**, *127*, 6506.
[80] M. Dincă, J. R. Long, *J. Am. Chem. Soc.* **2005**, *127*, 9376.
[81] S. S. Han, W. A. Goddard, III, *J. Am. Chem. Soc.* **2007**, *129*, 8422.
[82] Y. Li, R. T. Yang, *Langmuir* **2007**, *23*, 12937.
[83] Y. Y. Liu, Z. Ju-Lan, Z. Jian, F. Xu, L. X. Sun, *Int. J. Hydrogen Energy* **2007**, *32*, 4005.
[84] S. K. Bathia, A. L. Myers, *Langmuir* **2006**, *22*, 1688.
[85] M. Eddaoudi, J. Kim, N. Rosi, D. Vodak, J. Wachter, M. O'Keeffe, O. M. Yaghi, *Science* **2002**, *295*, 469.
[86] Y. Y. Sun, Y. H. Kim, S. B. Zhang, *J. Am. Chem. Soc.* **2007**, *129*, 12606.
[87] A. Mavrandonakis, E. Tylianakis, A. K. Stubos, G. E. Froudakis, *J. Phys. Chem. C* **2008**, *112*, 7290.
[88] A. Blomqvist, C. M. Araujo, P. Srepusharawoot, R. Ahuja, *Proc. Natl. Acad. Sci. U. S. A.* **2007**, *104*, 20173.
[89] G. Férey, F. Millange, M. Morcrette, C. Serre, M. L. Doublet, J. M. Greneche, J. M. Tarascon, *Angew. Chem. Int. Ed.* **2007**, *46*, 3259.
[90] B. Z. Fang, H. S. Zhou, I. Honma, *Appl. Phys. Lett.* **2006**, *89*, 023102.
[91] Y. Zhang, L. G. Scanlon, M. A. Rottmayer, P. B. Balbuena, *J. Phys. Chem. B* **2006**, *110*, 22532.
[92] K. L. Mulfort, J. T. Hupp, *Inorg. Chem.* **2008**, *47*, 7936.
[93] K. L. Mulfort, J. T. Hupp, *J. Am. Chem. Soc.* **2007**, *129*, 9604.
[94] M. Meilikhov, K. Yusenko, R. A. Fischer, *J. Am. Chem. Soc.* **2009**, *131*, 9644.
[95] Y. Li, R. T. Yang, *J. Am. Chem. Soc.* **2006**, *128*, 726.
[96] Y. Li, R. T. Yang, *J. Am. Chem. Soc.* **2006**, *128*, 8136.
[97] Y. W. Li, R. T. Yang, *AIChE J.* **2008**, *54*, 269.
[98] S. Proch, J. Herrmannsdörfer, R. Kempe, C. Kern, A. Jess, L. Seyfarth, J. Senker, *Chem. Eur. J.* **2008**, *14*, 8204.
[99] M. G. Nijkamp, J. E. M. J. Raaymakers, A. J. van Dillen, K. P. de Jong, *Appl. Phys. A* **2001**, *72*, 619.
[100] B. Panella, K. Hönes, U. Müller, N. Trukhan, M. Schubert, H. Pütter, M. Hirscher, *Angew. Chem. Int. Ed.* **2008**, *47*, 2138.
[101] T. Yildirim, M. R. Hartman, *Phys. Rev. Lett.* **2005**, *95*, 215504.
[102] S. Bordiga, J. G. Vitillo, G. Ricchiardi, L. Regli, D. Cocina, A. Zecchina, B. Arstad, M. Bjorgen, J. Hafizovic, K. P. Lillerud, *J. Phys. Chem. B* **2005**, *109*, 18237.
[103] J. L. C. Rowsell, J. Eckert, O. M. Yaghi, *J. Am. Chem. Soc.* **2005**, *127*, 14904.
[104] G. Garberoglio, *Langmuir* **2007**, *23*, 12154.
[105] A. Samanta, T. Furuta, J. Li, *J. Chem. Phys.* **2006**, *125*, 084 14.
[106] L. Zhang, Q. Wang, Y. C. Liu, *J. Phys. Chem. B* **2007**, *111*, 4291.
[107] T. Sagara, J. Klassen, E. Ganz, *J. Chem. Phys.* **2004**, *121*, 12543.
[108] E. C. Spencer, J. A. K. Howard, G. McIntyre, J. L. C. Rowsell, O. M. Yaghi, *Chem. Commun.* **2006**, 278.
[109] T. Sagara, J. Klassen, J. Ortony, E. Ganz, *J. Chem. Phys.* **2005**, *123*, 014701.
[110] Q. Y. Yang, C. L. Zhong, *J. Phys. Chem. B* **2005**, *109*, 11862.
[111] D. Kim, T. B. Lee, S. B. Choi, J. H. Yoon, J. Kim, S. H. Choi, *Chem. Phys. Lett.* **2006**, *420*, 256.
[112] J. L. Belof, A. C. Stern, M. Eddaoudi, B. Space, *J. Am. Chem. Soc.* **2007**, *129*, 15202.
[113] T. B. Lee, D. Kim, D. H. Jung, S. B. Choi, J. H. Yoon, J. Kim, K. Choi, S. H. Choi, *Catal. Today.* **2007**, *120*, 330.
[114] A. I. Skoulidas, D. S. Sholl, *J. Phys. Chem. B* **2005**, *109*, 15760.
[115] J. Liu, J. Y. Lee, L. Pan, R. T. Obermyer, S. Simizu, B. Zande, J. Li, S. G. Sankar, J. K. F. Johnson, *J. Phys. Chem. C* **2008**, *112*, 2911.
[116] F. Salles, H. Jobic, G. Maurin, M. M. Koza, P. L. Llewwellyn, T. Devic, C. Serre, G. Férey, *Phys. Rev. Lett.* **2008**, *100*, 245901.
[117] H. Frost, R. Q. Snurr, *J. Phys. Chem. C* **2007**, *111*, 18794.
[118] L. Pan, B. Parker, X. Huang, D. H. Olson, J. Y. Lee, J. Li, *J. Am. Chem. Soc.* **2006**, *128*, 4180.